

Evaporative Cooling in a Crossed Dipole Trap

Charles S. Adams, Heun Jin Lee, Nir Davidson, Mark Kasevich, and Steven Chu

Department of Physics, Stanford University, Stanford, California 94301

(Received 17 November 1994)

Laser cooled sodium atoms are trapped in an optical dipole force trap formed by the intersection of two $1.06\ \mu\text{m}$ laser beams. Densities as high as 4×10^{12} atoms/cm³ at a temperature of $\sim 140\ \mu\text{K}$ have been obtained in a $\sim 900\ \mu\text{K}$ deep trap. By reducing the trap depth over a 2 s interval, we have evaporatively cooled the atoms to a final temperature of $\sim 4\ \mu\text{K}$ at a density of 6×10^{11} atoms/cm³. This corresponds to a factor of 28 increase in atomic phase-space density.

PACS numbers: 32.80.Pj

Laser cooling and trapping techniques are capable of yielding dramatic increases in the phase-space density of dilute atomic vapors. For example, atoms from thermal atomic sources are routinely cooled and compressed in a magneto-optic trap (MOT) to densities of $\sim 10^{11}$ /cm³ and temperatures of $\sim 20T_{\text{rec}}$, where $k_B T_{\text{rec}} = (\hbar k)^2/2m$ is the photon recoil limit, k is the wave vector of the cooling laser, and m is the atomic mass [1]. Even higher phase-space densities are needed for the observation of quantum many body effects, such as Bose-Einstein condensation, and also for precision experiments requiring large fluxes of ultracold atoms.

Phase-space density in magneto-optic traps is constrained in temperature by the standard limits of polarization gradient cooling [2,3] and in density by radiative repulsion [4], light-assisted collisions [5], and the trap spring constant. Recent increases in MOT phase-space density have resulted from the development of improved techniques for minimizing the effects of radiative repulsion and light-assisted collisions, and the use of stronger magnetic trapping fields [6,7]. In this Letter, we report on the use of related techniques to achieve high densities at low temperatures in an optical dipole force trap, where we expect similar limiting mechanisms to be present.

We also report on the use of evaporative cooling to further increase the phase-space density in the trap [8]. Evaporative cooling was first demonstrated with magnetically trapped hydrogen [9] and has recently been observed with laser cooled, magnetically trapped alkali atoms [10,11]. Evaporative cooling is an attractive final stage cooling technique since, unlike laser cooling methods, it does not involve density limiting interactions with light. Successful evaporative cooling requires that the atom-atom elastic collision rate, which sets the time scale for thermalization in the trap dominate inelastic collision channels that can cause unwanted trap loss or heating. Two channels which are relevant to evaporation of sodium in optical dipole force traps are heating due to Rayleigh scattering of the trapping light and photoassociative two-body inelastic collisions [12,13]. In the work presented below, the use of far-detuned $1.06\ \mu\text{m}$ radiation for trapping minimizes both of these potentially adverse interactions.

Evaporative cooling in dipole traps offers flexibility in designing trap potentials, especially those with dynamically changing trap volume and depth. Crucially, such flexibility allows for optimization of the evaporative cooling path. In this proof-of-principle work, we cross two tightly focused laser beams to produce the trapping potential illustrated in Fig. 1. Previous dipole trapping work has been restricted to the use of a single tightly focused beam [14–16]. Our new geometry was chosen to give the trap a strong, nearly isotropic, spring constant and a relatively large volume. Trap depth, and to some extent trap volume, was changed by adjusting the intensity of the trapping beams.

We have recently demonstrated the efficacy of Raman cooling techniques for atoms confined in a single focus dipole force trap [17]. In this work we cooled the axial motion (parallel to the propagation vector of the dipole trapping beam) to an effective temperature of $0.7T_{\text{rec}}$. In the crossed dipole trap geometry, where the oscillation frequency of trapped atoms is balanced in all directions, we expect to be able to cool all three degrees of freedom. The use of a Raman cooling stage to precool an atomic sample in conjunction with a final evaporative cooling stage may provide access to even higher phase space densities.

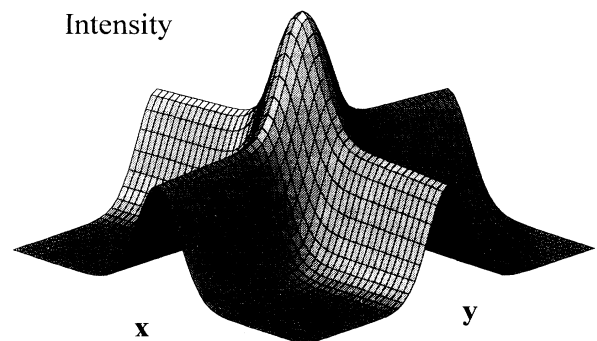


FIG. 1. A cross section of the dipole trap intensity distribution. The section plane is defined by the propagation axes of the two trapping beams, which are taken to be parallel x and y axes.

The experimental details are as follows [18]. Sodium atoms from a thermal atomic source were initially trapped and cooled in a MOT, which was then used to feed atoms into the crossed dipole trap. A 10 W single mode Nd:YAG laser generated the dipole trapping light. The laser output passed through an acousto-optic modulator, which provided electronic control of the intensity, before being divided into two independent beams. The trap was formed by intersecting these two beams at a 90° angle in the center of the MOT. Each beam had a measured $15 \mu\text{m}$ $1/e^2$ radius at the point of intersection and a maximum power of 4 W. The polarizations of the beams were chosen to be orthogonal in the crossed region in order to suppress standing wave effects. Under these conditions the maximum attainable trap depth was $\sim 900 \mu\text{K}$, much deeper than the $30 \mu\text{K}$ temperatures which are routinely achieved with polarization gradient molasses [2].

The dipole trap was loaded by leaving the dipole beams on at full power while loading atoms into the MOT. After a fixed loading interval (typically 2 s), the MOT beams and magnetic field were turned off, leaving atoms confined solely by the dipole trapping beams. The alignment of the trapping beams was optimized by maximizing the number loaded into the trap. The total number of atoms in the trap was measured by a probing the ensemble with laser light tuned to the $3S_{1/2} \rightarrow 3P_{3/2}$ transitions: After a fixed time following the shutoff of the MOT, the dipole beams were turned off and the light used to form the MOT was turned back on. Resonance fluorescence from the diffusively expanding ensemble of atoms was focused into a photomultiplier tube. Under the above static loading conditions, the number loaded into the trap was maximized for MOT beams of $\sim 3 \text{ mW}/\text{cm}^2$ peak intensity (intensity refers to total intensity in one of the six trapping beams), tuned -15 MHz below the $3S_{1/2}, F = 2 \rightarrow 3P_{3/2}, F = 3$ transition and a magnetic field gradient of $1 \text{ G}/\text{mm}$. To avoid optical pumping, a resonant electro-optic modulator imposed 1.73 GHz frequency sidebands on the MOT beams. One of these sidebands, whose power was 10% of that in the carrier, was nearly resonant with the $3S_{1/2}, F = 1 \rightarrow 3P_{3/2}, F = 2$ repumping transition. The number of atoms loaded into the dipole trap saturated for loading times $\sim 2 \text{ s}$, which also corresponds to the time necessary to saturate the number of atoms loaded into the MOT.

An order of magnitude more atoms were loaded into the trap by reducing the intensity of the repumping sideband by a factor of 16 during the final 20 ms of the trap loading interval. The overall effect of reducing the sideband intensity is to optically pump a greater fraction of the trapped atoms into the $F = 1$ ground state hyperfine level and reduce the excitation rate. Although we have not extensively studied the mechanism behind this increase in number, we conjecture that it results from a reduction in three density limiting processes: radiative repulsion forces [5], photo-associative

collisions, and ground state hyperfine changing collisions [19]. The first two processes are suppressed by the reduction of population in the $3P_{3/2}$ manifold. Although the 1.77 GHz energy exchange associated with the final process is not enough to eject atoms from the MOT, it will eject atoms from the dipole trap. Optical pumping into the $F = 1$ level minimizes population in the $F = 2$ level and therefore reduces this loss.

We measured the trap size by imaging fluorescence from the detection pulse onto a charge coupled device array. The imaging system had a $4.5\times$ magnification and a measured resolution of $\sim 3 \mu\text{m}$. The optical axis of the imaging system was normal to the plane containing both trapping beams as is illustrated in Fig. 2. For a total dipole trap power of 8 W, the measured $1/e$ half-width of a cross section passing through the center of the trap, at a 45° angle with respect to the trapping beams, was $7 \pm 2 \mu\text{m}$. For these measurements, the detection light had a $10 \text{ mW}/\text{cm}^2$ peak intensity per beam and was detuned -25 MHz from the cooling transitions. The diffusive spreading of the atomic cloud during the detection time was corrected for by measuring the size for 5 and $10 \mu\text{s}$ detection pulses. No corrections have been made for possible broadening of the imaging arising from the optical thickness of the sample.

The density in the dipole trap was determined by measuring the absorption of a weak probe beam. This beam was aligned to pass through the center of the crossed region as is illustrated in Fig. 2. The linearly polarized beam had a $7 \mu\text{m}$ $1/e^2$ waist and a power of $\sim 1 \text{ nW}$ to avoid saturation of the transition. The probe light was pulsed on for a $2 \mu\text{s}$ measurement interval following the extinction of the dipole trapping beams. This was short enough so that ballistic expansion of the atomic distribution during the measurement could be neglected. A plot of transmission against frequency is shown in Fig. 3. The three dips correspond to the $3S_{1/2}, F = 1$ to $3P_{3/2} F = 0, 1,$ and 2 transitions, respectively. The

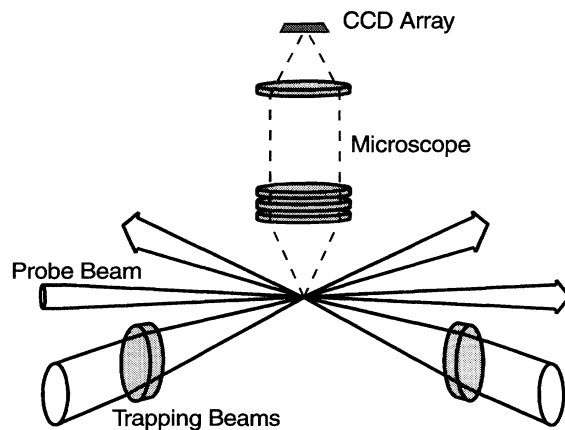


FIG. 2. Schematic illustration of the apparatus.

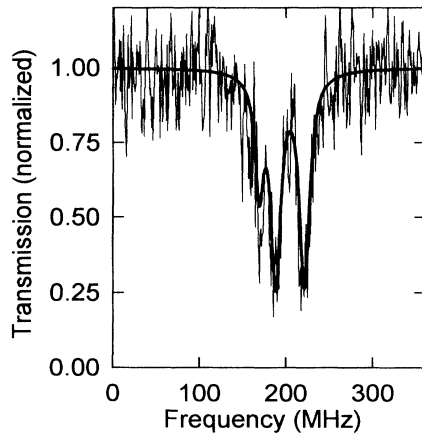


FIG. 3. Transmitted intensity as a function of probe laser frequency for a weak probe beam passing through the crossed region of the dipole trap. The solid curve is a fit of the modeled line shape to the data.

equal absorption on the $F = 1$ and $F = 2$ transitions indicates that the intensity and duration of the probe pulse were sufficiently small to avoid optical pumping of atoms into the $F = 2$ state. From the peak absorption of 75% and assuming a Gaussian atomic distribution $n = n_0 \exp(-r^2/r_0^2)$, where $r_0 = 7 \pm 2 \mu\text{m}$ was the measured $1/e$ radius of the atomic distribution, we calculate the peak density n_0 to be $4_{-2}^{+6} \times 10^{12}$ atoms/cm³ [20]. This measurement was also used to calibrate the sensitivity and collection efficiency of the video imaging system. Subsequent absolute density measurements were made with the video camera alone by inferring the number of trapped atoms from the integrated video signal and trap volume from the size measurement described above. The relative density in the crossed region was found to be an order of magnitude higher than the peak density in the trap wings.

The lifetime of the trap was measured by monitoring the number of atoms in the crossed region as a function of time. The lifetime data were fitted well by a single exponential decay, and were found to vary inversely with the trapping intensity and to be independent of the initial atomic number and density. At present we have no consistent explanation for the observed intensity and density dependence of the trap loss. The exponential decay time constant was 0.8 s for 8 W total trapping power and increased to 2.7 s for 2 W total power. For intensities less than 1 W, trap decay is dominated by background gas collisions. In the low intensity limit, the extrapolated lifetime is 14 s at our operating pressure of $\sim 6 \times 10^{-10}$ torr.

The temperature of atoms trapped in the crossed region was measured by a time-of-flight technique using the video imaging system. Images of the ballistically expanding ensemble were taken a fixed time delay after the dipole

trap was turned off. The delay was typically chosen to be long enough to allow the size of the ensemble to expand by roughly an order of magnitude over its initial size [21]. The effective temperature for atoms loaded into a $\sim 900 \mu\text{K}$ deep trap (corresponding to 8 W trapping power) was $140 \mu\text{K}$. From this measured temperature, we can use the virial theorem to estimate the expected spatial distribution of atoms in the trap. Modeling the trap potential in the central region as $V(x, y, z) = V_0\{\exp[-2(x^2 + y^2)/w_0^2] + \exp[-2(y^2 + z^2)/w_0^2]\}$ and the atomic density as $n(x, y, z) = n_0 \exp[-(x^2 + y^2 + z^2)/r_0^2]$ we calculate the expected $1/e$ radius to be $5.3 \mu\text{m}$, in rough agreement with the measured radius of $7 \pm 2 \mu\text{m}$.

We measured the heating rate due to off-resonant scattering of trap photons by observing the evolution of trap temperature with time in the deep (8 W) trap. The temperature in the crossed region was observed to increase at a rate corresponding to scattering one $1.06 \mu\text{m}$ photon every 0.8 s. This rate is consistent with the estimated photon scattering rate.

The atoms in the trap were evaporatively cooled by lowering the trapping potential. The Nd:YAG laser power was exponentially ramped down from 8 to 0.4 W in 2 s with a 0.7 s time constant. Examples of the video signal depicting the cooling sequence are shown in Fig. 4. Figure 4(a), which illustrates the change in trap density, was recorded with a $10 \mu\text{s}$ detection pulse applied immediately after the dipole trap was turned off. After the ramp the atomic density decreased by a factor of about $\sim 7 \times 10^{11}$ to $6_{-2}^{+6} \times 10^{11}$ atoms/cm³. Figure 4(b), which illustrates the change in trap temperature, shows the width of the atomic distribution following a $200 \mu\text{s}$ ballistic expansion interval. The half-width of the final velocity distribution $1/e$, was found to be 5.6 cm/s, which corresponds to a temperature of $4 \mu\text{K}$. Compared to the initial conditions, the ramp produced a 28-fold increase in the phase-space density of atoms in the crossed region of the trap, while the number of trapped atoms decreased from ~ 5000 to ~ 500 atoms.

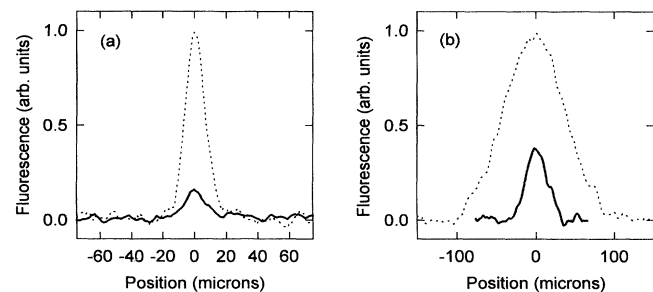


FIG. 4. (a) Image of trap size before (thin line) and after (thick line) the intensity ramp. (b) Time-of-flight measurement of trap temperature before (thin line) and after (thick line) the intensity ramp.

A fraction of the atoms which escape from the central region of the trap will remain confined by the wings of the dipole region. These atoms can return, in principle, to the central region of the trap, where they will collisionally heat the ensemble. However, a numerical simulation of single particle trajectories in the trap, which included both the light induced potential and the gravitational potential, indicated the probability of return to be less than 2% during the potential ramp. In addition, atoms which do return spend a relatively brief time in the central region before again escaping to the wings, further reducing the possibility of trap heating.

Recent experiments with magnetically trapped Na indicate an elastic collision cross section $\sim 10^{-12}$ cm² or larger for a sample in the $F = 1$, $m_f = +1$ state at a temperature of ~ 50 μ K [22]. For our initial trap density of 4×10^{12} atoms/cm³ and temperature of ~ 140 μ K, and assuming this cross section is a reasonable estimate for our unpolarized atomic sample, the collision rate is ~ 100 s⁻¹, giving an estimated rethermalization time $\sim 10^{-1}$ s [23,24]. At the end of the ramp, this time is ~ 1 s. Experimentally, the 0.7 s ramp time constant gave optimal cooling results, and is roughly consistent with this estimate.

Although this represents a clear demonstration of evaporative cooling, the process is far from optimized. The rapid evaporation and rethermalization which occurs during the initial stages of the ramp soon shut off due to the loss of density as the potential relaxes. Efficient evaporative cooling would require simultaneous evaporation and compression, which we plan to implement in subsequent experiments.

We wish to thank E. Cornell, J. Doyle, W. Ketterle, and C. Wieman for useful discussions, and M. Perry for his loan of a Nd:YAG laser. C. S. A. acknowledges the support of the English Speaking Union. This work was supported in part by grants from the NSF and the AFOSR.

-
- [1] E. Raab, M. Prentiss, A. Cable, S. Chu, and D. Pritchard, Phys. Rev. Lett. **59**, 2631 (1987).
 - [2] For discussions of polarization gradient cooling limits, see Special issue on *Laser cooling and trapping*, edited by S. Chu and C. E. Wieman [J. Opt. Soc. Am. B **6**, (1989)].
 - [3] A. Steane and C. Foot, Europhys. Lett. **14**, 231 (1991).
 - [4] T. Walker, D. Sesko, and C. Wieman, Phys. Rev. Lett. **63**,

- 957 (1989); D. Sesko, T. Walker, and C. Wieman, J. Opt. Soc. Am. B **8**, 946 (1991).
- [5] D. Sesko, T. Walker, C. Monroe, A. Gallagher, and C. Wieman, Phys. Rev. Lett. **63**, 961 (1989).
- [6] W. Petrich *et al.*, J. Opt. Soc. Am. B **11**, 1332 (1994).
- [7] W. Ketterle, K. Davis, M. Joffe, A. Martin, and D. Pritchard, Phys. Rev. Lett. **70**, 2253 (1993).
- [8] H. Hess, Phys. Rev. B **34**, 3476 (1986).
- [9] N. Masuhara *et al.*, Phys. Rev. Lett. **61**, 935 (1988).
- [10] K. Davis, M. Mewes, M. Joffe, and W. Ketterle, in *Atomic Physics 14*, edited by C. Wieman and D. Wineland (AIP, New York, 1994).
- [11] W. Petrich, M. Anderson, J. Ensher, and E. Cornell, in *Atomic Physics 14* (Ref. [10]).
- [12] P. Lett *et al.*, Phys. Rev. Lett. **71**, 2200 (1993).
- [13] J. Miller, R. Cline, and D. Heinzen, Phys. Rev. Lett. **71**, 2204 (1993).
- [14] S. Chu, J. Bjorkholm, A. Ashkin, and A. Cable, Phys. Rev. Lett. **57**, 314 (1986).
- [15] J. Miller, R. Cline, and D. Heinzen, Phys. Rev. A **47**, R4567 (1994).
- [16] S. Rolston *et al.*, Proc. SPIE **1726**, 205 (1992).
- [17] H. J. Lee, C. S. Adams, N. Davidson, B. Young, M. Weitz, M. Kasevich, and S. Chu, in *Atomic Physics 14* (Ref. [10]).
- [18] A detailed description of our trapping apparatus can be found in M. Kasevich and S. Chu, Appl. Phys. B **54**, 321 (1992).
- [19] See, for example, P. Julienne, A. Smith, and K. Burnett, in *Advances in Atomic, Molecular, and Optical Physics*, edited by B. Bederson and H. Walther (Academic Press, San Diego, 1992); T. Walker and P. Feng, in *Advances in Atomic Molecular, and Optical Physics*, *ibid.*
- [20] The density was calculated by integrating over the finite size of the probe beam and using the absorption cross section for linearly polarized light resonant with the $3S_{1/2}$ $F = 1$ to $3P_{3/2}$ $F = 2$ transition, $\frac{5}{6}\lambda^2/2\pi$, where λ is the transition wavelength.
- [21] Atoms from the wings of the distribution contribute to the ballistic expansion signal. We have made a Monte Carlo simulation of the atomic distribution following the ballistic expansion interval in order to assess the impact of the contribution on the measured temperature. We find that the wing atoms increase the width of the final distribution by $\sim 5\%$.
- [22] W. Ketterle (private communication).
- [23] This estimate assumes the collision cross section for the $m_f = 0$ state to be comparable to that of the $m_f = \pm 1$ state.
- [24] Results for the rethermalization of ultracold Cs appeared in C. Monroe, E. Cornell, C. Sackett, C. Myatt, and C. Wieman, Phys. Rev. Lett. **70**, 414 (1993).

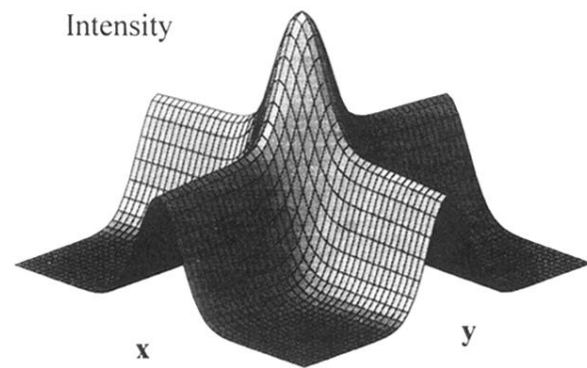


FIG. 1. A cross section of the dipole trap intensity distribution. The section plane is defined by the propagation axes of the two trapping beams, which are taken to be parallel x and y axes.